Electronic Supplementary Material (ESI) for Dalton Transactions.

MOF crystal growth: UV resonance Raman investigation of metal-ligand binding in solution and accelerated crystal growth methods

Thomas D. Petersen[a], Gurusamy Balakrishnan[b], Colin L. Weeks[a,*]

[a]Department of Chemistry and Biochemistry, University of Northern Iowa, Cedar Falls, IA, 50614, USA

[b]Department of Chemistry, University of Washington, Seattle, WA, 98195, USA

Supplementary Data

Slow Diffusion Crystal Growth Reactions

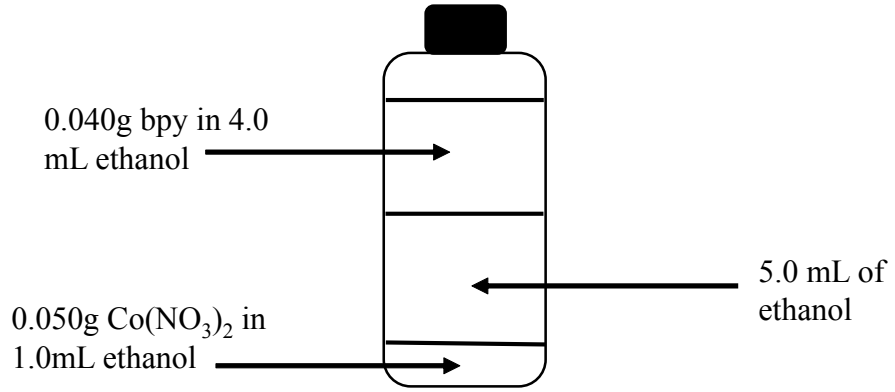

Figure S1. Schematic diagram of the vial set up for diffusion reactions of $Co(NO_3)_2$ and bpy to grow the 2D bilayer crystals of $[Co_2(bpy)_3(NO_3)_4]_n$.

Raman Spectra

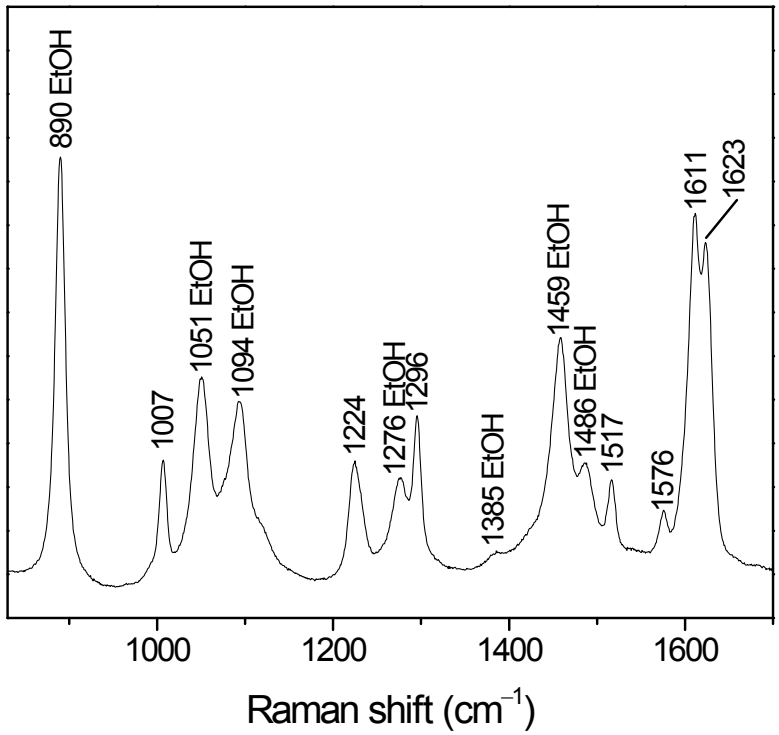

Figure S2. Raman spectrum of 1.0 mM bpy in ethanol obtained using 229 nm excitation.

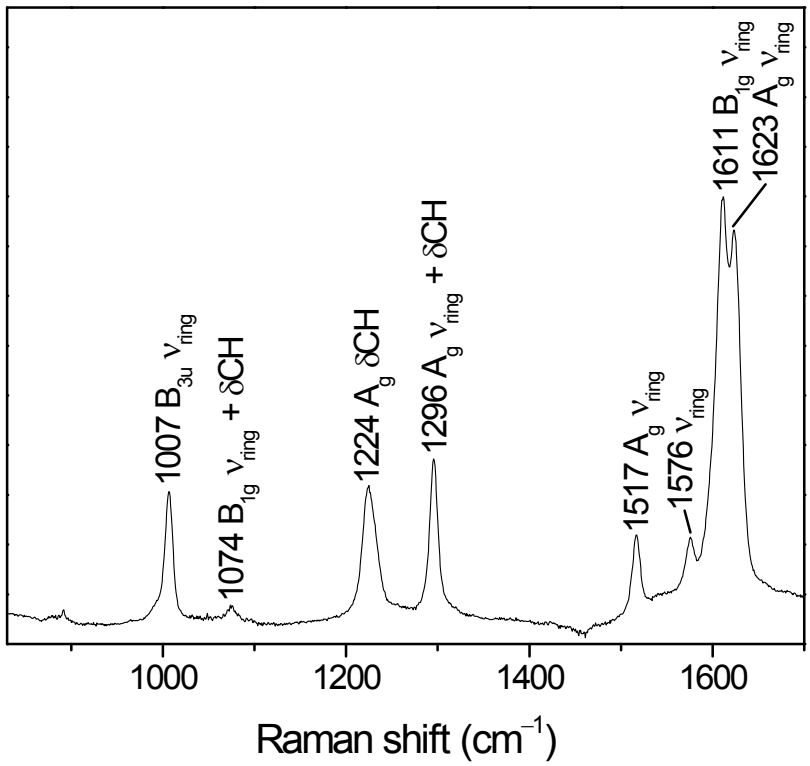

Figure S3. Raman spectrum of 1.0 mM bpy in ethanol obtained using 229 nm excitation after subtraction of the contribution of the ethanol bands.

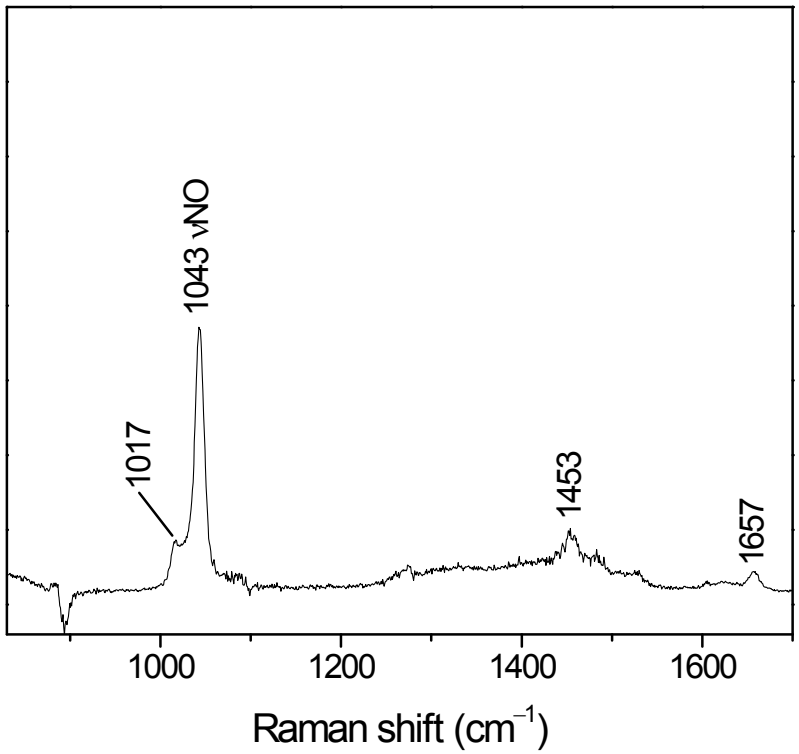

Figure S4. Raman spectrum of 1.0 mM $Co(NO_3)_2$ in ethanol. Ethanol bands subtracted, λ_{ex} = 229 nm.

Table S1. Comparison of band fitting parameters for the bpy vibrational bands in the Raman spectrum before and after subtracting the contribution of the bands from the ethanol solvent.

Band assignment[a]	1.0 mM bpy in ethanol		1.0 Mm bpy in ethanol spectrum – ethanol spectrum	
	band position[b] (cm^{-1})	band width (cm^{-1})	band position[b] (cm^{-1})	band width (cm^{-1})
B_{3u} ν_{ring}	1006.5	10.3	1006.7	9.8
B_{1g} ν_{ring} + δCH	1077.2	15.5	1074.0	21.1
A_g δCH[c]	1222.9	10.7	1222.7	14.1
	1226.8	19.3	1230.3	14.9
A_g ν_{ring} + δCH	1295.8	9.1	1295.6	10.3
A_g ν_{ring}	1517.0	11.0	1516.6	10.2
ν_{ring}	1574.9	10.0	1575.0	11.1
B_{1g} ν_{ring}	1610.5	18.7	1610.5	19.2
A_g ν_{ring}	1625.4	13.5	1625.5	13.5

[a] Bands assigned according to references [1] and [2].

[b] The fitted band positions of some vibrational modes differ slightly from the intensity maxima labeled on the spectra due to the sloping background created by partial overlap with nearby peaks.

[c] Fitting showed that the 1224 cm^{-1} peak in the experimental spectrum required two bands (one at 1222.9 cm^{-1} and a second at 1226.8 cm^{-1} or 1230.3 cm^{-1}) to accurately produce the slightly unsymmetrical peak shape. Either of these component bands could correspond to the previously reported A_g δCH band in this region of the bpy spectrum.

UV-vis Spectra

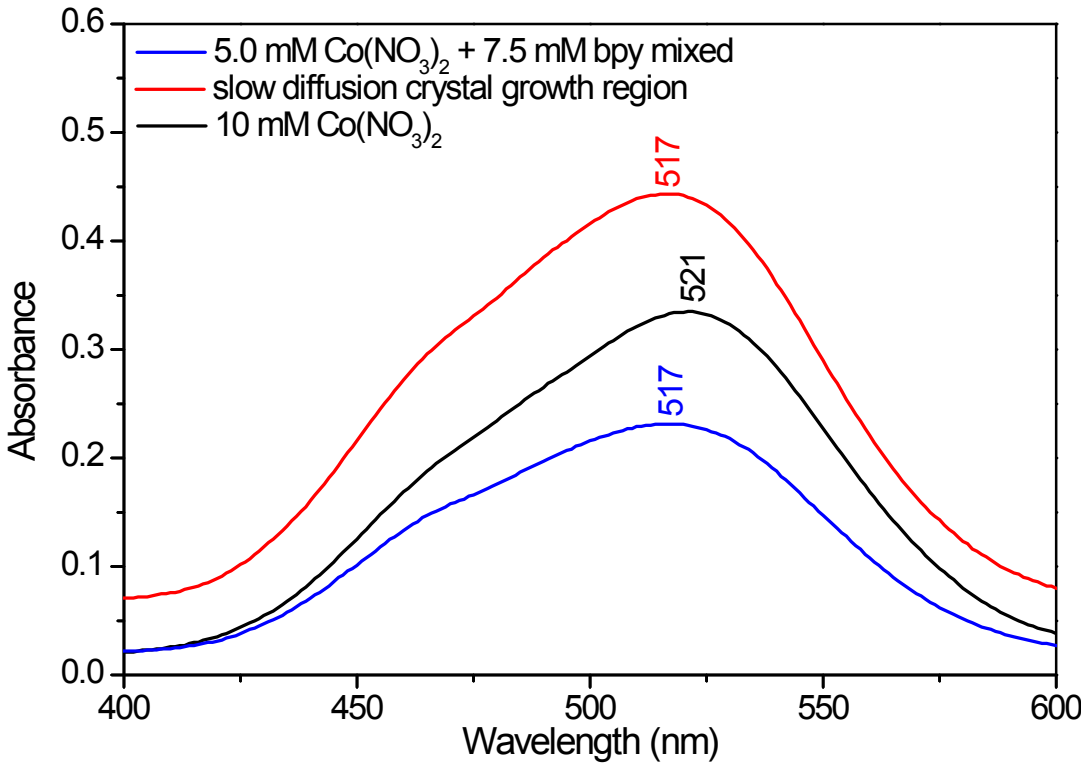

Figure S5. UV-visible spectra of the solution from the region of the vial in which the 2D bilayer crystals were growing after slowly diffusing for 1 day and the 5.0 mM $Co(NO_3)_2$ + 7.5 mM bpy solution produced by direct mixing. The spectrum of 10 mM $Co(NO_3)_2$ in ethanol is also shown for comparison.

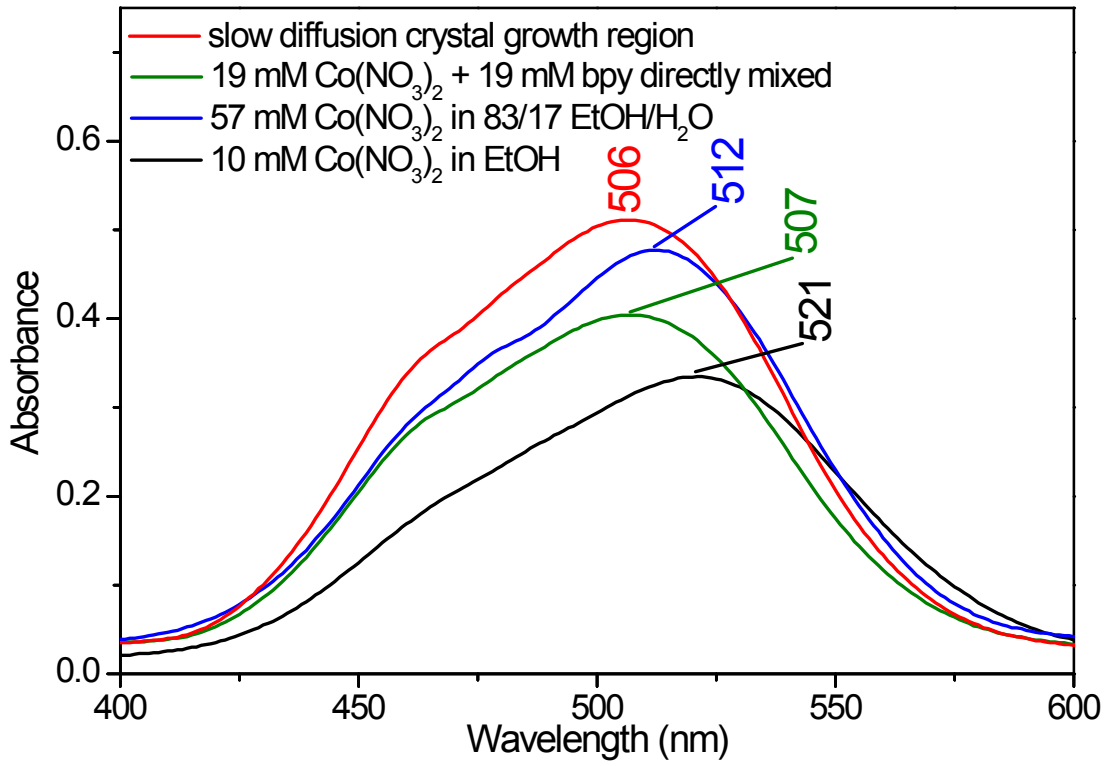

Figure S6. UV-visible spectra of the solution from the region of the vial in which the 1D chain crystals were growing after slowly diffusing for 3 days and the 19 mM $Co(NO_3)_2$ + 19 mM bpy solution produced by direct mixing 3 min after mixing. The spectra of 10 mM $Co(NO_3)_2$ in ethanol and 57 mM $Co(NO_3)_2$ in ethanol/water (83/17 v/v) are also shown for comparison.

The shift of the absorbance maximum from 521 nm in ethanol solution of $Co(NO_3)_2$ to 512 nm in the ethanol/water solution of $Co(NO_3)_2$ showed that in the latter solution more water ligands were bound to the Co^{2+} as water is a stronger field ligand than ethanol or nitrate. The further blue-shift of the absorbance maximum in the solutions from the crystal growth region of the slow diffusion reaction and in the direct mixing of $Co(NO_3)_2$ and bpy solutions showed that bpy was coordinating to the Co^{2+} in solution.

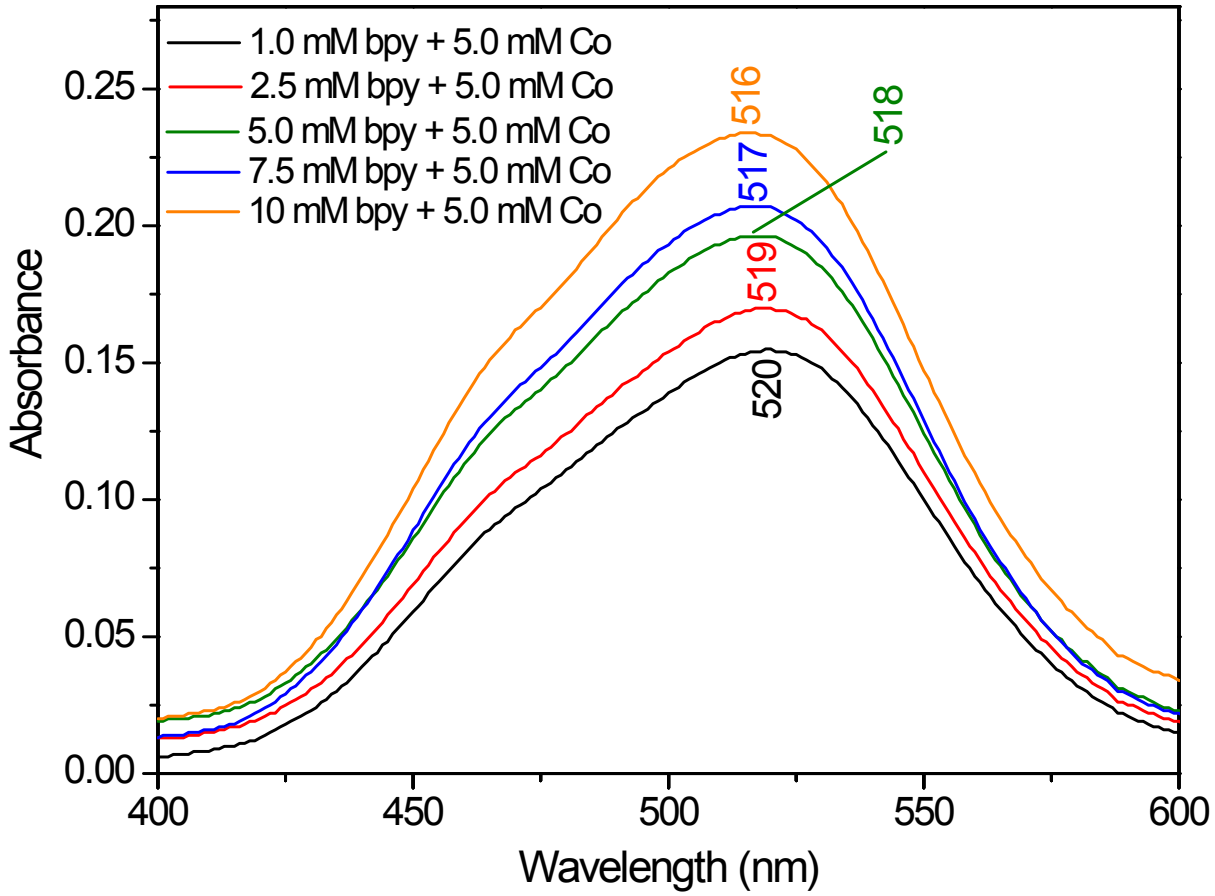

Figure S7. UV-visible spectra of the solutions produced by direct mixing of 5.0 mM $Co(NO_3)_2$ and varying bpy concentrations in ethanol The spectra were recorded immediately after mixing.

The concentration of bpy could not exceed 10 mM because at higher bpy concentrations crystal formation started before the UV-visible spectrum could be recorded. The λ_{max} of the Co $d \rightarrow d$ transition showed a monotonic decrease as the Co:bpy ratio decreased from 5:1 to 1:2. Since λ_{max} was changing over the whole range of Co:bpy ratios that could be tested it was not possible to determine the stoichiometry of the major soluble Co^{2+}-bpy species that formed in solution. The gradual, continual decrease in λ_{max} over the whole range of Co:bpy ratios indicated that more than one soluble Co^{2+}-bpy species was present in solution as the bpy:Co^{2+} ratio varied.

Slow Diffusion vs Direct Mixing Crystal Formation of 1D Chain MOF

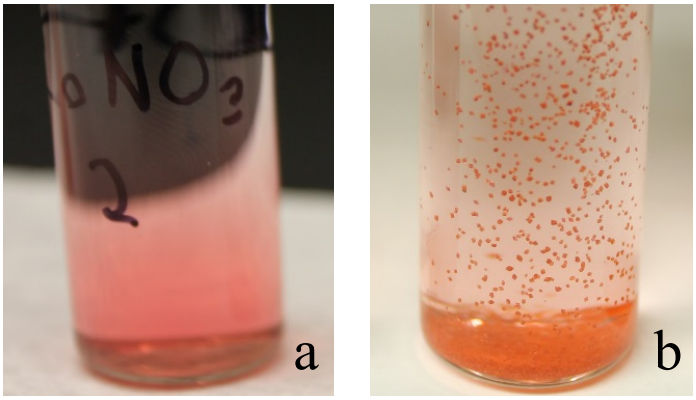

Figure S8. a) Slow diffusion reaction of 1D chain crystals after 1 day showing the absence of crystal formation b) 1D chain crystals formed 1 day after direct mixing of $Co(NO_3)_2$ and bpy solutions in ethanol/water.

Powder X-ray Diffraction Patterns

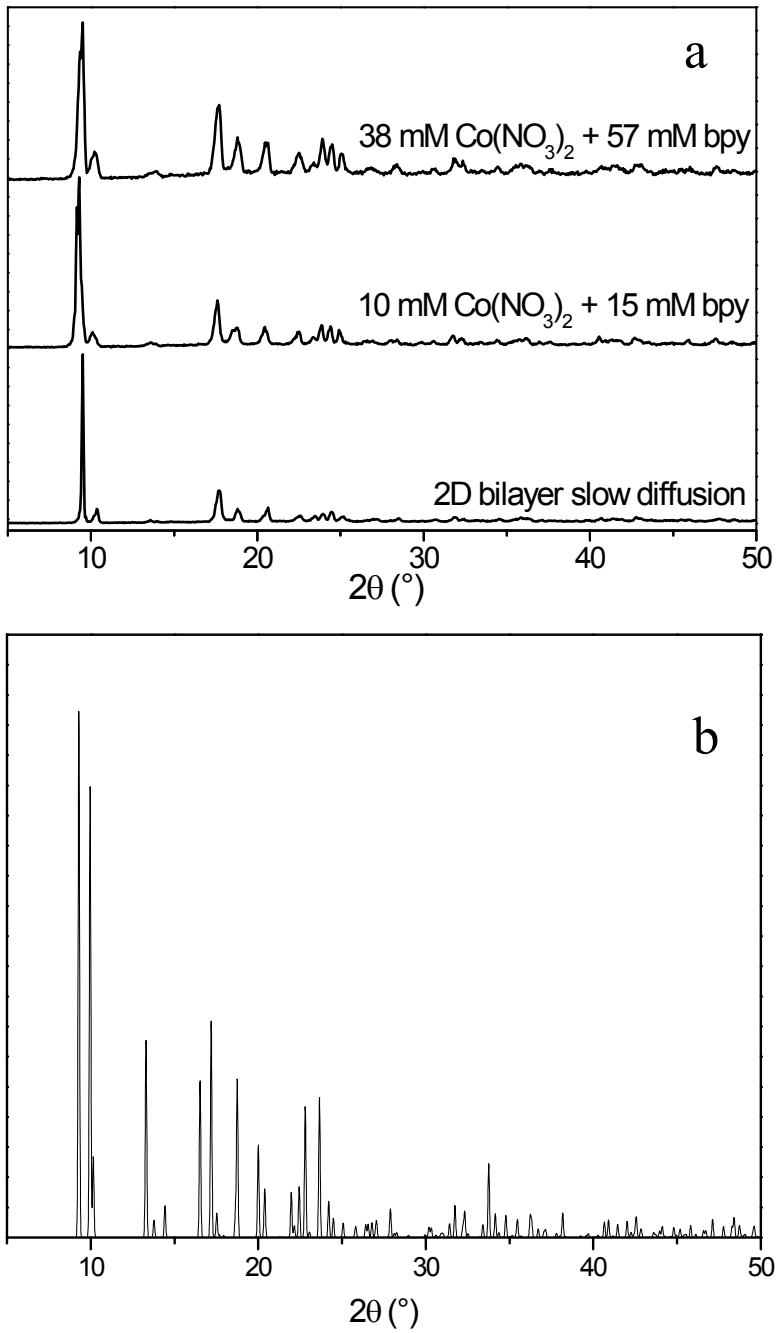

Figure S9. a) Experimental PXRD pattern for samples of 2D bilayer crystals prepared by direct mixing and slow diffusion, b) Simulated PXRD pattern calculated using Crystal Diffract[3] from the CCDC-100382 CIF file for the 2D bilayer crystals.[4]

Table S2. Comparison of 2θ values of the peaks from the powder X-ray diffraction patterns of the 2D bilayer crystals with the peak positions predicted for the simulated powder patterns calculated using Crystal Diffract[3] from the CCDC-100382 CIF file for the 2D bilayer crystals.[4]

Experimental 2D bilayer Direct mixing sample 10 mM $Co(NO_3)_2$ + 15 mM bpy		Experimental 2D bilayer Slow diffusion sample		Simulated from SCXRD data		
2θ (°)	Relative intensity (%)	2θ (°)	Relative intensity (%)	2θ (°)	Relative intensity (%)	*hkl*
9.3	100	9.5	100	9.3	100	0 2 0
10.1	11.8	10.4	8.2	10.0 10.2	85.9 15.3	1 1 1 0 0 2
13.6	1.9	13.6	1.5	13.3 13.8	37.6 3.3	1 1 2 0 2 2
17.6	25.1	17.7	17.7	17.2 17.5	41.2 4.7	2 2 0 1 1 3
18.8	9.8	18.8	7.3	18.7	30.0	1 3 2
20.5	10.0	20.6	7.9	20.4	9.3	0 0 4
22.5	7.1	22.6	3.0	22.4	9.7	0 2 4
23.4	3.8	23.5	2.8			
23.8	11.1	24.0	4.0	23.7	26.5	2 4 0
24.4	10.3	24.5	5.3	24.2 24.5	6.9 3.7	2 4 1 3 1 2
24.9	8.3	25.2	2.9	25.0	2.7	2 0 4
26.6	1.6			26.4 26.6	2.5 2.6	3 3 1 1 5 2
26.9	2.1	27.0	1.3	27.1	2.8	3 1 3
28.0	2.0			27.9	5.5	3 3 2
28.4	2.7	28.5	1.7	28.3	0.9	2 4 3
29.9	1.4			30.0	0.6	0 6 2
30.6	1.9	30.7	0.9	30.3 30.6	1.8 0.4	3 1 4 4 2 0
31.8	5.0	31.9	2.5	31.7	6.1	2 6 0
32.3	3.5	32.4	1.4	32.3	4.9	4 2 2
33.4	1.1	33.2	0.6	33.4	2.4	2 6 2
34.4	2.3	34.6	1.3	34.2 34.4	3.1 0.9	2 0 6 4 2 3
		35.6	1.2	35.5	3.3	2 2 6
		35.8	2.1	35.7	0.3	1 5 5
36.2	3.5	36.3	1.8	36.2 36.3	4.0 3.0	0 4 6 4 4 2
37.6	1.4	37.6	0.3	37.8	0.8	0 8 0
39.6	0.9	39.8	0.7	39.6	0.4	1 3 7
40.5	4.7	40.7	1.6	40.6	2.8	3 3 6
41.3	2.9	41.4	0.7	41.5	2.4	0 0 8

41.7	2.1	41.9	1.0	42.0	3.1	2 8 2
42.7	3.4	42.8	2.1	42.5 42.6	1.9 2.7	5 1 4 0 2 8
43.5	1.6			43.6	0.9	2 4 7
45.9	2.6	46.0	0.7	45.8	2.3	0 4 8
47.6	3.2	47.8	1.1	47.8	1.9	0 10 0
48.5	1.6			48.39 48.40 48.42	1.8 1.0 1.1	4 8 0 1 9 4 6 4 0
		48.7	0.9	48.7	1.0	3 9 1
49.9	1.4	50.0	0.7	49.8	0.2	1 3 9
51.0	0.9			51.0	0.8	1 9 5

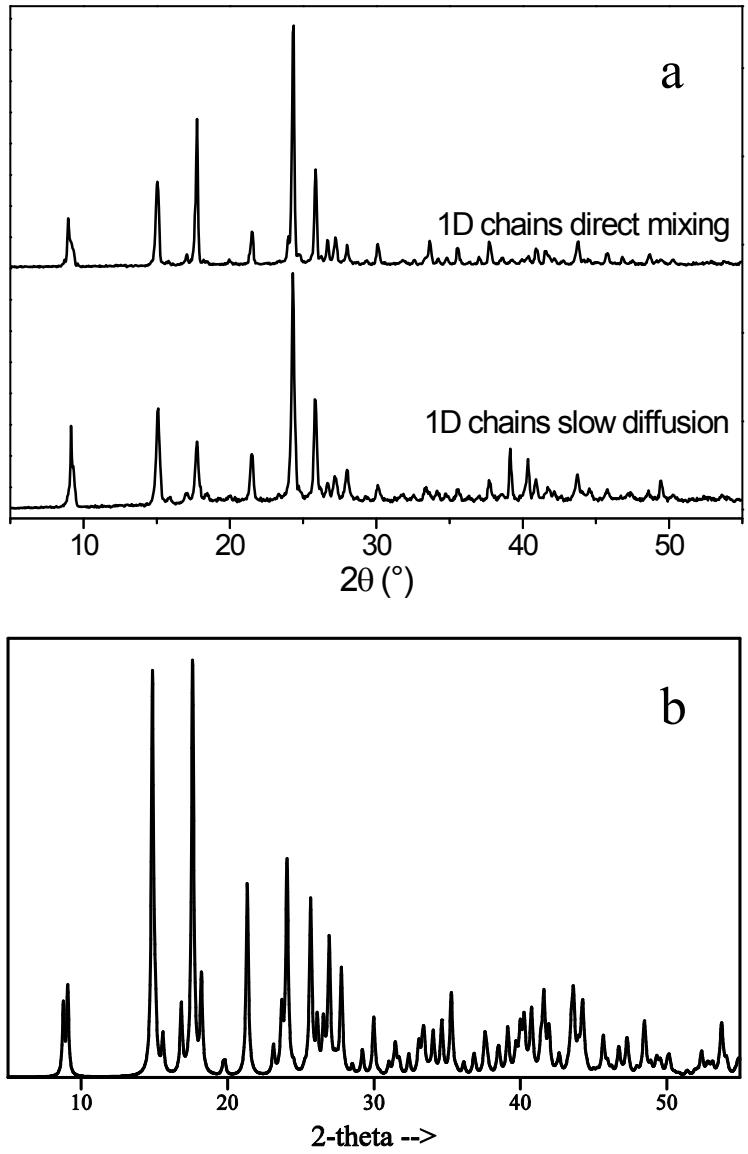

Figure S10. a) Experimental PXRD pattern for samples of 1D chain crystals prepared by direct mixing and slow diffusion, b) Simulated PXRD pattern calculated using XPREP[5] from the SCXRD *hkl* reflection data for the 1D chain crystals.[6]

Table S3. Comparison of 2θ values of the peaks from the powder X-ray diffraction patterns of the 1D chain crystals with the peak positions predicted for the simulated powder patterns calculated using XPREP[5] from the SCXRD *hkl* reflection data for the 1D chain crystals.[6]

Experimental 1D chains Direct mixing sample		Experimental 1D chains Slow diffusion sample		Simulated from SCXRD data		
2θ (°)	Relative intensity (%)	2θ (°)	Relative intensity (%)	2θ (°)	Relative intensity (%)	*hkl*
9.0	20.2	9.2	36.4	8.8 9.1	20.0	1 1 0 0 2 0
15.0	35.2	15.1	42.5	14.9	96.1	1 1 1
17.0	4.2	17.1	4.5	16.8	17.9	1 2 1
		17.7	27.9	17.6	99.1	2 2 0
		18.4	4.5	18.2	25	0 4 0
		19.3	2.2			
20.0	1.8	20.0	3.4	19.8	4.2	2 1 1
21.5	13.9	21.5	20.7	21.3	45.8	2 2 1
		23.3	1.6	23.1	7.9	1 4 1
24.3	100	24.3	100	24.05 24.08	51.7	1 5 0 0 0 2
25.8	39.0	25.8	43.7	25.7	42.6	1 1 2
26.7	8.1	26.7	5.0	26.5 25.6	15.0	3 3 0 2 4 1
27.2	10.5	27.2	8.5	27.3	6.7	3 2 1
28.0	7.5	28.0	12.4	27.8	26.2	0 3 2
29.3	1.5	29.3	2.0	29.2	6.6	3 3 1
30.1	8.6	30.1	6.7	30.0	14.2	2 2 2
31.8	1.6	31.8	2.4	31.68 31.73 31.78	4.9	3 4 1 2 3 2 4 2 0
32.6	1.6	32.5	2.2	32.4	5.6	3 5 0
33.6	9.6	33.4	5.5	33.3 33.4	9.1	3 0 2 0 5 2
34.2	2.0	34.2	3.5	34.04 34.06	11.2	2 4 2 4 2 1
34.8	2.6	34.8	2.8	34.59 34.63	13.6	3 2 2 3 5 1
35.6	6.8	35.6	4.5	35.3	20.0	1 7 1
37.0	3.0	37.0	2.0	36.82 36.84 36.90	5.7	2 5 2 0 6 2 0 8 0
37.8	9.4	37.7	8.8	37.6 37.7	10.8	1 1 3 1 6 2
38.6	2.4	38.6	1.7	38.4 38.5	7.5	1 2 3 5 1 0
39.3	1.5	39.2	22.3	39.1	11.9	4 0 2

40.4	2.2	40.4	16.3	40.26 40.29	15.4	4 2 2 4 5 1
40.9	5.9	40.9	7.2	40.75 40.76 40.78	16.6	3 5 2 2 2 3 5 3 0
41.6	5.1	41.7	3.9	41.6	20.7	3 7 1
42.2	2.3			42.0	12.7	2 8 1
42.7	1.4	42.6	1.6	42.6	5.8	5 3 1
43.8	8.9	43.7	10.3	43.6 43.7	21.7	3 1 3 3 6 2
		44.6	3.6			
45.8	4.4	45.8	4.3	45.66 45.70	10.0	3 3 3 5 0 2
46.8	2.8			46.61 46.69 46.73	7.3	0 10 0 5 2 2 5 5 1
47.5	1.3	47.4	3.0	47.28 47.28 47.39	9.4	2 8 2 6 2 0 3 4 3
48.7	3.8	48.6	3.7	48.41 48.46 48.51	13.4	4 1 3 4 6 2 4 8 0
49.4	1.6	49.4	8.1	49.25 49.31 49.38 49.39	5.2	2 10 0 0 0 4 5 6 1 1 9 2
50.3	1.9	50.3	2.0	50.15 50.18 50.25	5.5	4 8 1 1 1 4 0 2 4
		53.6	1.8	53.60 53.74 53.74 53.77	12.9	1 4 4 1 10 2 6 2 2 1 11 1

References

(1) Caswell, D. S.; Spiro, T. G. *Inorg. Chem. Commun.* **1987**, *26*, 18.
(2) Topaçli, A.; Akyüz, S. *Spectrochim. Acta* **1995**, *51A*, 633.
(3) CrystalMaker Software Ltd.; 6.0.3 ed.; CrystalMaker Software Ltd: Begbroke, UK, 2014, Calculation and simulation of diffraction patterns
(4) Kondo, M.; Yoshitomi, T.; Seki, K.; Matsuzaka, H.; Kitagawa, S. *Angew. Chem., Int. Ed. Engl.* **1997**, *36*, 1725.
(5) BrukerAXS; Bruker Analytical X-ray Instruments Inc.: Madison, Wisconsin, USA, 1995.
(6) Mauger-Sonnek, K.; Streicher, L. K.; Lamp, O. P.; Ellern, A.; Weeks, C. L. *Inorg. Chim. Acta* **2014**, *418*, 73.